Available online at www.sciencedirect.com

ScienceDirect

Energy Procedia 129 (2017) 1141–1148

Energy Procedia

www.elsevier.com/locate/procedia

IV International Seminar on ORC Power Systems, ORC2017
13-15 September 2017, Milano, Italy

Fluid-dynamic design and characterization of a mini-ORC turbine for laboratory experiments

M. Pini[a,*], C. De Servi[b], M. Burigana[a], S. Bahamonde[a], A. Rubino[a], S. Vitale[a], P. Colonna[a]

[a]*Delft University of Technology, Aerospace Engineering Faculty, Propulsion and Power, Kluyverweg 1, 2629 HS Delft,The Netherlands*
[b]*Flemish Institute for Technology Research (VITO), Boeretang 200, Mol 2400, Belgium*

Abstract

High temperature Organic Rankine Cycles power systems of low power capacity, i.e. 3-50 kW_e, are receiving recognition for distributed and mobile energy generation applications. For this type of power plants, it is customary to adopt a radial-turbine as prime mover, essentially for their ability to cope with very large volumetric flow ratio with limited fluid-dynamic penalty. To date, the design of such turbines is based on design guidelines and loss models developed mainly for turbo-chargers, subsequently adapted by means of non-validated computational fluid-dynamic calculations. In the attempt to provide data sets for CFD validation and calibration of loss models, a mini-ORC radial inflow turbine delivering $10kW$ of mechanical power will be realized and tested in the Propulsion and Power Laboratory of TU-Delft. The fluid dynamic design and characterization of the machine is detailed in this paper. According to available models, the results indicate that the optimal layout of mini-ORC turbines can substantially differ from that of radial-inflow turbines utilized in more traditional applications, strengthening the need of experimental campaigns to support the conception of new design practices.

Peer-review under responsibility of the scientific committee of the IV International Seminar on ORC Power Systems.

Keywords: mini-ORC turbines; radial-inflow turbine; CFD; Loss Breakdown

Nomenclature

η_{ts}	total-to-static efficiency
Ω	rotational speed
P_0	inlet total pressure
T_0	inlet total temperature
VR	volumetric flow ratio
$\Delta\alpha$, $\Delta\beta$	stator / rotor flow deflection
$Mach_{\text{stator, rotor}}$	Mach number at stator outlet or rotor inlet

* Corresponding author. Tel.: +31 (0)15 27 84794 .
E-mail address: m.pini@tudelft.nl

1876-6102
Peer-review under responsibility of the scientific committee of the IV International Seminar on ORC Power Systems.
10.1016/j.egypro.2017.09.186

1. Introduction

High-speed mini-turbines are utilized to generate mechanical power in high-temperature Organic Rankine Cycle turbogenerators of power capacity in the 3-50 kW range [1]. In the vast majority of cases, these machines are of radial-inflow type, due to their compactness, high power density and capability to operate at high flow coefficients. The combined effect of high-pressure ratios and the low speed of sound, peculiar of organic compounds, leads to single-stage machines constituted by a supersonic radial stator vane and a transonic mixed-flow rotor. Moreover, the design is further complicated by their small dimensions, which make tip-leakage flow and viscous effects comparatively more relevant than in larger ORC machines. Achieving high efficiency is therefore particularly challenging and conventional design rules developed for turbochargers are arguably not applicable to mini-ORC radial-inflow turbines. Presently, the optimal design of this type of expanders is executed by means of non-validated tools applied in the preliminary and detailed design phase. Therefore, the estimated performance of mini-ORC turbines designed with either meanline or computational fluid dynamic models might considerably deviate from the actual value, making the real net conversion efficiency of mini-ORC generators uncertain.

To bridge the above mentioned knowledge gap, a high-speed (~100 krpm) mini-ORC radial-inflow turbine operating with siloxane MM will be constructed and tested in the ORCHID facility [2] at the Propulsion and Power Laboratory of Delft University of Technology. The main aim is to measure the actual fluid-dynamic performance of mini-ORC expanders and, evenly important, to create a set of data for i) validating CFD tools; ii) validating CFD-based design methodologies; and iii) calibrating loss correlations to enhance the reliability of preliminary design methods. The validated tools will be subsequently used to define new design practices for mini-ORC turbines.

The design process and the layout of the machine is documented in this paper and its fluid-dynamic performance are investigated by means of three-dimensional Reynolds-Averaged Navier-Stokes (RANS) calculations. Eventually, a loss breakdown is provided to gain insight into the principal loss mechanisms in mini-ORC radial-inflow turbines and first design guidelines are drawn on the basis of physical understanding.

2. Turbine layout

The first step of the design process of a turbomachine is the selection of its configuration (e.g. axial, radial-inflow, radial-outflow). This selection is usually performed by means of statistical diagrams, e.g. the Balje's charts, which relate the machine efficiency to the specific speed N_s and specific diameter D_s. For small-scale unconventional turbomachinery applications, like the ORC turbine under investigation, the use of such diagrams, essentially developed for incompressible flow machines, is somewhat questionable and may lead to erroneous choices [3]. To overcome this issue, the choice of the best turbine configuration for ORC systems has to rely on more sophisticated methodologies that are able to consider non-ideal and compressible flow effects in the assessment of the turbine performance. Recent work [4] outlined that for low power capacity ORC systems (order of 10 kW_e) the radial-inflow turbine architecture is the most promising, essentially for the ability to accommodate high volumetric flow ratio in a single stage with reduced rotor tip leakage losses if compared to axial and radial-outflow configurations. For this reason, the radial-inflow turbine has been selected as the candidate turbo-expander for the first experimental campaign in the ORCHID facility.

2.1. Meanline turbine design

The meanline design of the turbine has been accomplished by means of the integrated design methodology proposed in [4], whereby the optimal preliminary fluid dynamic design of the turbine is performed simultaneously with the optimal design of the thermodynamic cycle. The main characteristics of the turbo-expander are summarized in Table 1a, whereas the meridional section of the turbine and the underlying thermodynamic cycle layout are shown in Figure 1. The total-to-static efficiency of the expander has been predicted by using the loss model documented in [5]. The estimated conversion efficiency of the ORC systems, which adopts siloxane MM as working fluid, exceeds 22%.

η_{ts}	83%
$\dot{W}$	12 kW
Ω	98 krpm
P_0	18.1 bar
T_0	300°C
P_s	0.443 bar
VR	46
$\Delta\alpha$	78°
$\Delta\beta$	90°
$Mach_{\text{stator,rotor}}$	1.9, 0.5

(a)

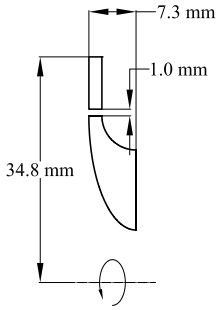

(b)

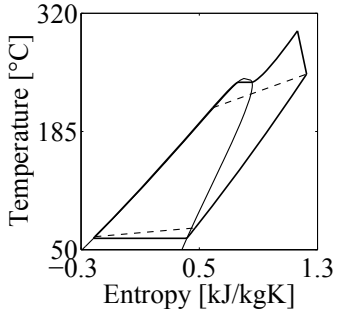

(c)

Fig. 1: (a) Main characteristics of the mini-ORC turbine operating with siloxane MM. (b) Meridional section of the mini-ORC radial-inflow turbine. (c) T-s diagram of the thermodynamic cycle.

2.2. Definition of the stator and rotor blading

The design of the blades of a mini-ORC RIT poses specific challenges; the stator is highly supersonic and the shape of the diverging part of the nozzle as well as that of the semi-bladed region is crucial to avoid the onset of strong shock waves [6]. At the same time, the flow in the rotor is transonic and is subject to a deflection exceeding 90°, resulting in comparatively large over-speed on the blade suction side that may eventually trigger flow separation. Notice that the optimal solution found through the meanline code features a back-swept angle at the rotor inlet to minimize incidence losses. The diverging portion of the stator has been designed using the method of characteristics (MoC) for non-ideal flows adapted to radial vanes. The prescribed Mach number at the outlet section of the diverging channel, needed to obtain the channel profile through MoC, has been determined at meanline design level by using the empirical model proposed in [7], which provides the optimal area ratio of the diverging part to minimize fluid-dynamic losses arising from viscous and post-expansion effects. A first tentative rotor endwall contour has been accomplished by following the design guidelines provided in [8], which suggests a 90° circular and a 90° elliptic arc for the shroud and the hub, respectively. On the contrary, the camberline curvature has been retrieved by imposing a linear variation of the blade metal angle between the inlet and the outlet ones. Figure 2a displays the resulting stator and rotor configuration.

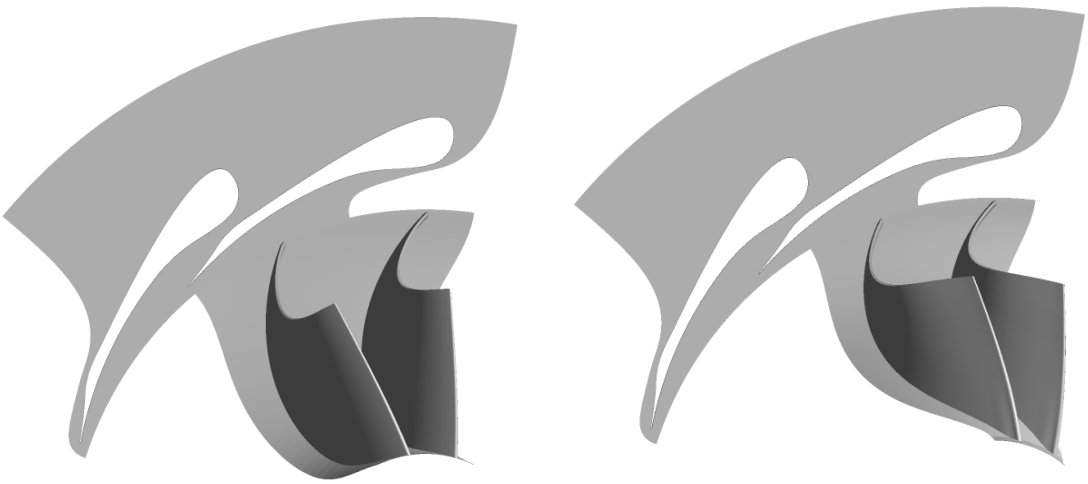

(a) (b)

Fig. 2: Schematic of the turbine configuration: (a) Baseline geometry (b) Optimized geometry

As shown in the following, the baseline turbine geometry, obtained with the above-mentioned guidelines, is refined by means of shape optimization.

3. Numerical assessment of the candidate turbine

3.1. Numerical model

The fluid-dynamic performance of the turbine have been assessed by means of a three-dimensional steady-state CFD model developed in the commercial Ansys solver CFX 17.1 [9]. The mixing-plane interface has been used to transfer the flow quantities between the stator and the rotor. Despite unsteady effects have been found to largely affect the flow distribution in radial ORC machines [10], the mixing-plane model has been proved suitable to predict the turbine total-to-static efficiency with an average discrepancy of about 0.5 percentage points against the experimental datum in more conventional radial-turbine applications [12]. The thermo-physical properties of the siloxane MM have been computed via a tabulated approach, in which the thermodynamic and transport property values are calculated by using the Span-Wagner's and Chung's model available in FluidProp [11]. Turbulence effects have been modeled by the Shear-Stress Transport (SST) closure. The mesh cells have been clustered such that $y^+ < 1$ along the blade surface and $y^+ < 5$ on the endwalls. An initial grid independence study was carried out to identify the most suitable mesh size. Figure 3 shows the trend of the total-to-static efficiency as a function of the mesh cells number. For the purpose of this work, the mesh with 3.5 million elements has been deemed sufficiently accurate. All the calculations have been run with a high-order resolution scheme for the advective and turbulent fluxes.

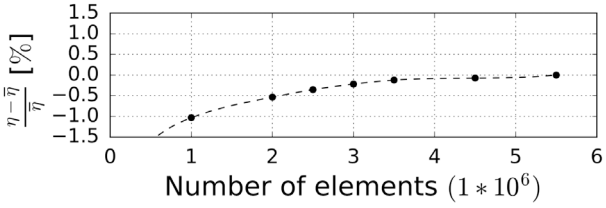

Fig. 3: Grid independence study, shown in terms of normalized total-to-static efficiency. The reference value is the one with 5.5 million cells.

3.2. Results of the baseline turbine configuration

Figure 4 depicts the Mach number and the normalized entropy contours at mid-span for the baseline configuration. According to CFD calculations, the turbine features a η_{ts} of 79.4%. At nearly 0.25% of the camberline length, the flow separates on the suction side due to the excessive streamwise adverse pressure induced by the uniform curvature of the camberline. This low momentum flow, along with the vorticity due to the blade surface boundary layers, is then transported radially outward by the radial component of the Coriolis force and by the spanwise pressure gradient caused by the curvature of the meridional plane. The flow leaking from the tip-clearance has the net effect to enhance the accumulation of low momentum flow close to the shroud which eventually mixes-out with the core flow downstream of the trailing-edge, see Figure 5. The final result is the appearance, at the exducer exit section, of a region of non-uniform, higher entropy flow on the portion of suction side from mid-span to shroud, while the rest of the flow is almost loss free. Conversely, the entropy generation in the supersonic stator is mainly caused by the wake, whereas the entropy jump across shock-waves, not noticeable in the entropy contour, seems to be, at least qualitatively, much less important.

3.3. Optimization of the rotor geometry

The previous results were insightful to provide directions about the geometry modifications to the original rotor shape. One key-parameter to control the magnitude and the extent of flow diffusion on the suction side is the flow passage area distribution. In radial-to-axial impellers, the actual flow passage area is determined by the shape of

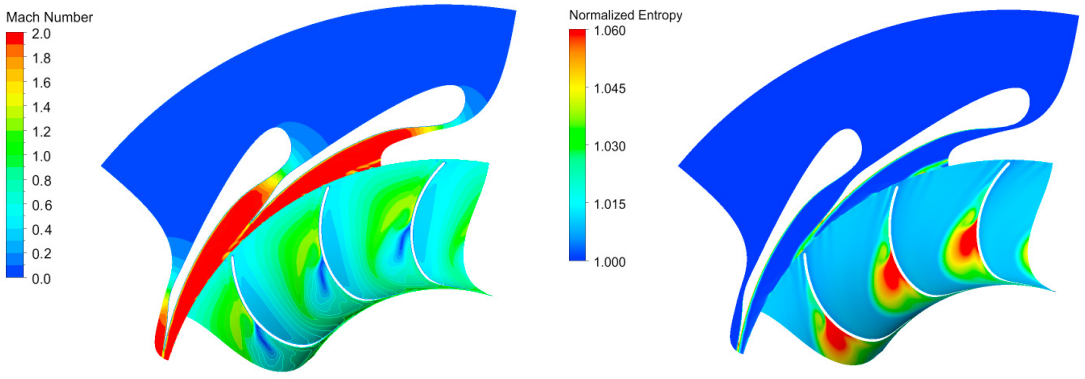

(a) (b)

Fig. 4: Baseline turbine configuration: (a) Mach number contour at mid-span (b) Normalized entropy contour at mid-span.

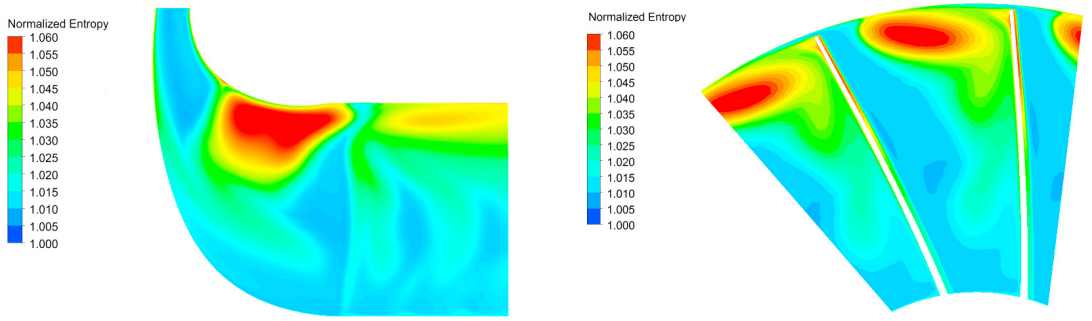

(a) (b)

Fig. 5: Baseline turbine configuration: (a) Normalized entropy contour on the meridional streamsurface (b) Normalized entropy contour at the exducer outlet section.

the sole meridional channel and by the azimuthal blade spacing, which is ultimately a function of the camberline curvature and blade solidity. Unlike in fully radial impellers, in which geometry modifications of the meridional channel only can be sufficient to obtain significant fluid-dynamic benefits [12], in back-swept rotors the blade-to-blade area distribution is expected to have comparatively large impact on the aerodynamic blade loading, thus loss generation, and should be a variable of the design process. Furthermore, it is envisaged that back-swept rotors require a higher number of blades than that needed in wheels with fully radial entry. Hence, the optimal blade solidity arguably differs with respect to the optimal value given by the meanline design. Stemming from these considerations, the rotor has been redesigned by applying surrogate-based shape optimization. The support vector machine regression technique available in [9] has been used to build the response surface. Shroud tip has been assumed to reduce the computational burden of the optimization. Preliminary calculations revealed that the accuracy of the response surface considerably deteriorates when the meridional channel shape and camberline profile are considered concurrently in the design process. Therefore, the optimization problem has been divided in three different, subsequent, sub-problems, namely:

1. optimization of the hub and shroud of the meridional channel;
2. optimization of the camberline profile at hub and shroud;
3. optimization of the rotor solidity, i.e. blade count, and spanwise angle distribution.

The maximization of the turbine total-to-static efficiency, i.e. $\eta_{ts} = \frac{h_{01}-h_{02}}{h_{01}-h_{2is}}$, has been chosen as objective function. The parametrization of the impeller has been defined by using 3^{rd} order Bezier curves. The degrees of freedom of the control points are indicated by the arrows in Figure 6. In the 2^{nd} optimization step, the control points marked in red have been considered, while in the 3^{rd} step the position of the first and last control point of the camberline is varied. Proper constraints have been set to avoid unfeasible geometries. The three response surfaces have been constructed by using 55, 44, and 44 samples, respectively. Figure 2b shows the optimized turbine layout.

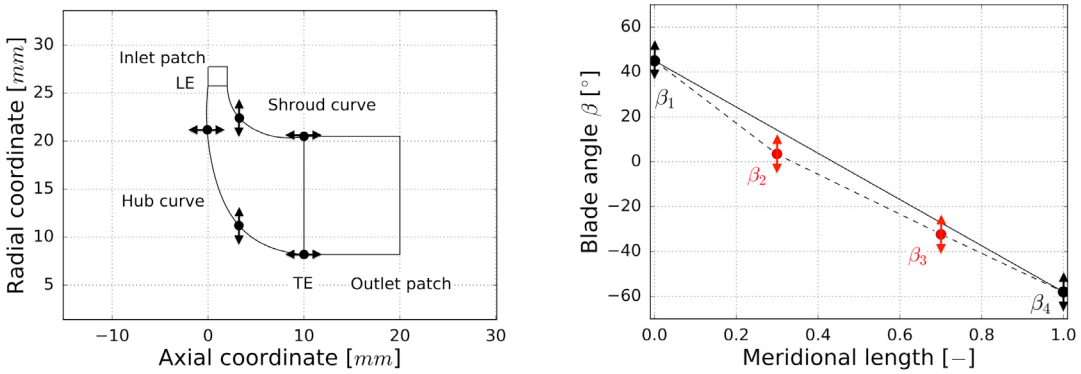

(a) (b)

Fig. 6: Geometry parametrization: (a) Parametrization of the meridional channel (b) Parametrization of the camberline profile.

3.4. Results of the optimized turbine configuration

The Mach and entropy contours are displayed in Figure 7 for the optimized turbine configuration, which features a η_{ts} of 80.8% assuming a tip gap of $\frac{1}{20}$ of the inlet blade height. As can be observed, the re-designed meridional channel is characterized by a smoother transition of the meridional flow passage area between the inlet and the outlet section, see Figure 8. The optimization of the camberline has lead to a more front-loaded profile, of similar shape at hub, mid, and tip section. Most of the flow deflection occurs now in the inducer, i.e. the radial part of the rotor channel. Yet, the number of blades has increased, passing from 15 to 19. The net effect of these geometrical changes is the reduction of the aerodynamic blade loading which is essential to attenuate the flow diffusion over the suction side and to prevent flow separation up to the tip. A large portion of the exducer exit is still interested by secondary and tip vortex flow, see Figure 8, which are then expected to have substantial impact on the fluid-dynamic performance of the impeller.

3.5. Loss breakdown

A loss breakdown has been finally performed to gain insight of the principal loss mechanisms occurring in mini-ORC radial-inflow turbines. Figure 9 shows the various loss contributions, expressed as a deficit in total-to-static efficiency. The following entropy generation mechanisms have been considered, i) viscous dissipation in boundary layers and dissipation across shock waves on the blade surfaces ii) mixing-out of the trailing-edge wake, boundary layers, and shock waves downstream of the cascade iii) viscous dissipation on the endwalls and mixing enhancement due to secondary flow iv) mixing-out of the tip leakage flow within the core flow. The losses of the groups i) and ii) have been determined by performing two-dimensional calculations at mid-span and by averaging the flow quantities at three different locations (e.g. inlet, immediately downstream the trailing-edge, and outflow boundary). The efficiency drop due to the dissipation along the blade surfaces is associated to the entropy increase between inlet and the trailing-edge, whereas the drop from the trailing-edge to the outlet boundary is related to mixing losses.

In both turbine configurations, the fluid-dynamic losses in the stator are significantly larger than those in the rotor, confirming the results found in [12] for a medium power capacity ORC radial-inflow turbine. Especially for the stator,

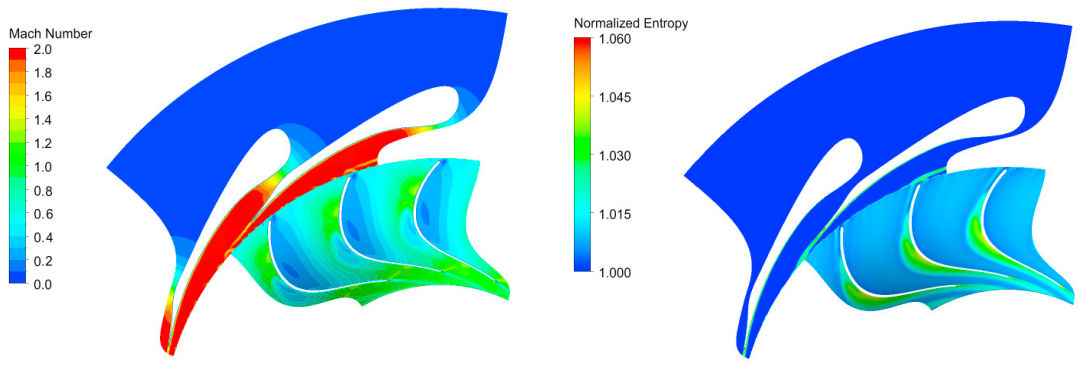

Fig. 7: Optimized turbine configuration: (a) Mach number contour at mid-span (b) Entropy contour at mid-span.

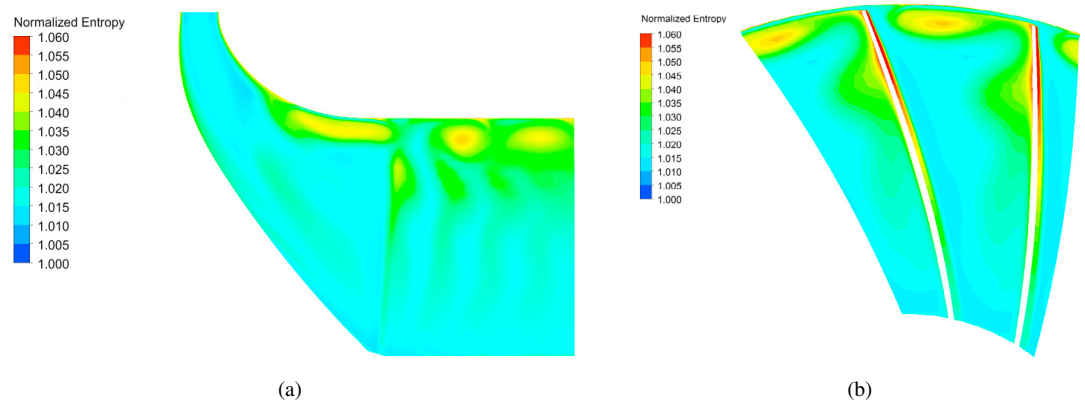

Fig. 8: Optimized turbine configuration: (a) Entropy contour on the meridional streamsurface (b) Entropy contour at the exducer outlet section.

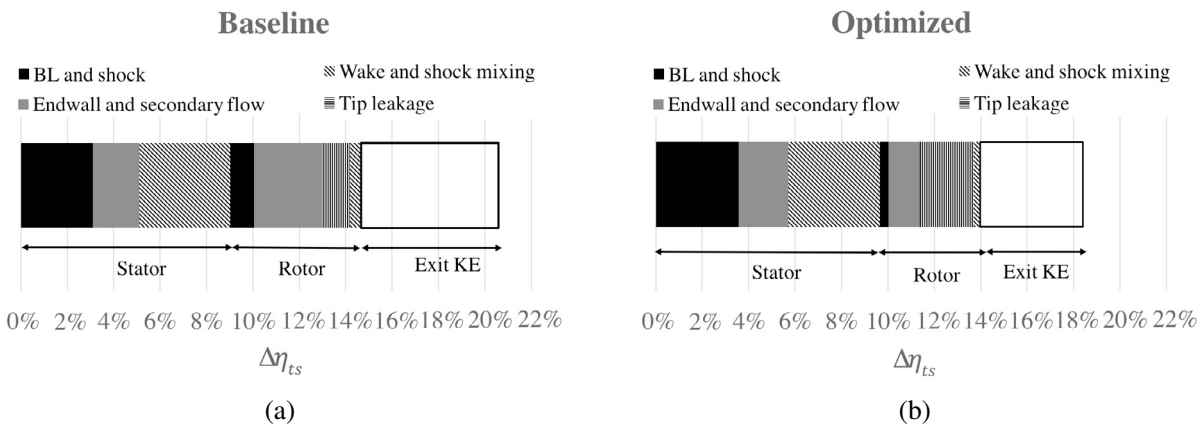

Fig. 9: Loss breakdown: (a) Baseline turbine configuration (b) Optimized turbine configuration.

the major loss contribution is due to the wake mixing downstream of the vane trailing-edge. The rotor suffers from severe fluid dynamic penalty due to endwalls dissipation, secondary flow-induced mixing and tip leakage flow. This suggests the importance of properly sealing the blade tip gap in mini-ORC turbines to contrast this latter loss source.

Notice that the rotor shape optimization, by relieving the amount of flow diffusion on the blade suction side, enabled to mitigate not only the entropy generation along the blade surfaces. Thanks to that, it reduces also the secondary flow induced by the convection of the boundary layers vorticity from the blade surface to the secondary plane resulting from the action of the Coriolis force and the meridional streamwise pressure gradient. From a general standpoint, the viscous dissipation on the walls is responsible for at least 40% of the total-to-static efficiency deficit, meaning that the accurate modeling of the flow characteristics within boundary layers, especially in non-ideal flow conditions, is of paramount importance for reliable efficiency prediction of mini-ORC radial-inflow turbines.

4. Conclusions

The detailed design and the characterization of the fluid dynamic performance of a mini-ORC radial inflow turbine have been documented in this paper. The efficiency of the first machine layout, whose geometry has been developed based on the results of a meanline model, has been increased by 1.5 percentage points reshaping the impeller via CFD-based automated design. According to steady CFD, the final configuration features a total-to-static efficiency of approximately 81% assuming unshrouded rotor. The results of this work outlined that current design rules for radial-inflow turbines are arguably not applicable to mini-ORC turbines and new design guidelines must be devised. As opposed to conventional radial-inflow machines, the stator suffers from higher fluid-dynamic losses and most of the entropy generation derives from viscous dissipation in the boundary layers. Instead, the rotor efficiency debit can be chiefly attributed to endwall and tip-leakage effects. Further efficiency reduction is envisaged due stator-rotor interaction and this is the focus of ongoing work. Finally, the uncertainty related to the characteristics of the boundary layers and associated amount of dissipation, especially in non-ideal conditions, demands for experimental confirmation.

Acknowledgments

The authors greatly acknowledge the Dutch Technology Foundation STW and the partner Robert Bosch GmbH (grant number 13385) and DANA Holding Corporation (grant number 12171) for funding this work.

References

[1] Colonna, P., Casati, E., Trapp, C., Mathijssen, T., Larjola, J., Turunen-Saaresti, T., et al. Organic rankine cycle power systems: From the concept to current technology, applications, and an outlook to the future. Journal of Engineering for Gas Turbines and Power 2015;137(10):100801–100801–19. URL: http://dx.doi.org/10.1115/1.4029884.

[2] Head, A.J., De Servi, C., Casati, E., Pini, M., Colonna, P.. Preliminary design of the orchid: A facility for studying non-ideal compressible fluid dynamics and testing orc expanders. ASME Turbo Expo: Power for Land, Sea, and Air 2016;(49743):V003T25A001–. URL: http://dx.doi.org/10.1115/GT2016-56103.

[3] Macchi, E., Perdichizzi, A.. Efficiency prediction for axial-flow turbines operating with nonconventional fluids. Journal of Engineering for Power 1981;103(4):718–724. URL: http://dx.doi.org/10.1115/1.3230794.

[4] Bahamonde, S., Pini, M., De Servi, C., Rubino, A., Colonna, P.. Method for the preliminary fluid dynamic design of high-temperature mini-orc turbines. Journal of Engineering for Gas Turbines and Power 2017;:–URL: http://dx.doi.org/10.1115/1.4035841.

[5] Qiu, X., Baines, N.. Performance prediction for high pressure-ratio radial inflow turbines. ASME Turbo Expo: Power for Land, Sea, and Air 2007;(47950):945–956. URL: http://dx.doi.org/10.1115/GT2007-27057.

[6] Pini, M., Persico, G., Pasquale, D., Rebay, S.. Adjoint method for shape optimization in real-gas flow applications. Journal of Engineering for Gas Turbines and Power 2014;137(3):032604–032604–13. URL: http://dx.doi.org/10.1115/1.4028495.

[7] Deych, M.Y., Troyanovskiy, B.. Investigation and calculation of axial turbine stages. Tech. Rep.; US Air Force; 1964.

[8] Glassman, A.. Computer program for design analysis of radial-inflow turbines. Tech. Rep.; NASA Lewis Research Center; 1976.

[9] Ansys® workbench, release 17.1, ansys, inc. 2017.

[10] Rinaldi, E., Pecnik, R., Colonna, P.. Unsteady operation of a highly supersonic organic rankine cycle turbine. Journal of Turbomachinery 2016;138(12):121010–121010–9. URL: http://dx.doi.org/10.1115/1.4033973.

[11] Colonna, P., van der Stelt, T., Guardone, A.. Fluidprop (version 3.0): A program for the estimation of thermophysical properties of fluids. Tech. Rep.; Delft University of Technology; 2014.

[12] Wheeler, A.P.S., Ong, J.. A study of the three-dimensional unsteady real-gas flows within a transonic orc turbine. ASME Turbo Expo: Power for Land, Sea, and Air 2014;(45660):V03BT26A003–. URL: http://dx.doi.org/10.1115/GT2014-25475.